Nano Research

Open Access

Research Article

Largely enhanced out-of-plane electromechanical coupling effects in two-dimensional molybdenum-disulfide/boron-nitride heterostructures

Qiong Liu[1,2], Vijay Kumar Choyal[1], James E. Morris[3], Timon Rabczuk[4], Xiaoning Jiang[5], and Xiaoying Zhuang[1,6,7] ✉

[1] *Institute of Photonics (IOP), Faculty of Mathematics and Physics, Leibniz University Hannover, Hannover 30167, Germany*
[2] *Laboratory of Nano and Quantum Engineering (LNQE), Leibniz University Hannover, Hannover 30167, Germany*
[3] *Department of Electrical & Computer Engineering, Portland State University, Portland, OR 97207-0751, USA*
[4] *Institute of Structural Mechanics, Bauhaus University, Weimar 99423, Germany*
[5] *Department of Mechanical and Aerospace Engineering, North Carolina State University, Raleigh, NC 27695-7910, USA*
[6] *Department of Geotechnical Engineering, College of Civil Engineering, Tongji University, Shanghai 200092, China*
[7] *Cluster of Excellence PhoenixD (Photonics, Optics and Engineering – Innovation Across Disciplines), Hannover 30167, Germany*

Cite this article: *Nano Research*, **2025**, *18*, 94907050. https://doi.org/10.26599/NR.2025.94907050

ABSTRACT: The electromechanical coupling effects in two-dimensional (2D) transition metal dichalcogenides (TMDs) have attracted great interest. However, for 2D TMDs, piezoelectricity is confined to the basal plane, and the flexoelectricity-derived out-of-plane electromechanical response is usually faint, limiting the applications of this material family using the out-of-plane electromechanical effects. Here, this work reports a facile strategy to greatly enhance the out-of-plane electromechanical response of hexagonal molybdenum disulfide (2H-MoS_2) nanoflakes by stacking monolayer hexagonal boron nitride (h-BN) on 2H-MoS_2 nanoflakes to form MoS_2/BN heterostructures. The d_{33}^{eff} coefficient of MoS_2/BN can reach a value comparable to that of commonly used wurtzite bulk piezoelectric materials, such as AlN and GaN. The strong out-of-plane electromechanical response of MoS_2/BN is due to the breaking of the out-of-plane structural symmetry. Kelvin probe force microscopy (KPFM) results show an increased effective work function of MoS_2/BN, indicating polar-structure formation at the heterostructure interface, which also accounts for the enhanced out-of-plane piezoresponse. This study gives an insight into the role of heterostructure engineering in the electromechanical performances of 2D TMDs, and provides this material family an opportunity for applications using out-of-plane electromechanical effects.

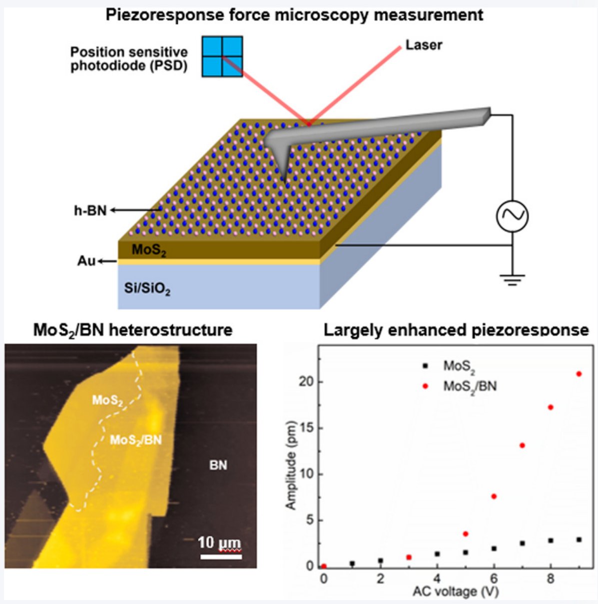

KEYWORDS: transition metal dichalcogenides, two-dimensional heterostructures, flexoelectricity, out-of-plane electromechanical coupling, symmetry breaking

1 Introduction

Electromechanical coupling, the coupling of electronic and mechanical properties, is of great importance in dielectric materials.

Received: August 5, 2024; **Revised:** September 22, 2024
Accepted: September 24, 2024

✉ Address correspondence to zhuang@iop.uni-hannover.de

Materials with electromechanical coupling effects have been widely applied in nanogenerators [1], microelectromechanical systems (MEMS) [2], actuators [3], and sensors [4]. Two-dimensional (2D) van der Waals (vdW) materials beyond graphene have attracted tremendous attention due to their unique physical properties and functions [5, 6]. They are ideal platforms to study electromechanical coupling due to their exceptional flexibility. Miniaturization of functional devices can be achieved by taking advantage of their 2D nature. Thus, great interest has been raised to study the electromechanical properties of 2D vdW materials [7, 8].

Monolayer or few-layered hexagonal 2D transition metal dichalcogenides (TMDs) with trigonal prismatic crystal structures have been proven to possess in-plane piezoelectricity due to the broken inversion symmetry [9]. However, the lack of out-of-plane mirror asymmetry for TMDs results in the absence of out-of-plane piezoelectric polarizations, which limits their applications using out-of-plane electromechanical coupling effects. Another important electromechanical coupling is flexoelectricity, which is a phenomenon that describes the polarization formation under a strain gradient. Flexoelectricity exists in all kinds of dielectric materials regardless of their central symmetry [10–12]. Flexoelectricity-derived out-of-plane electromechanical responses have been found in various 2D TMDs [11], whereas most 2D TMDs have an out-of-plane electromechanical response noncomparable to that of commonly used piezoelectric bulk materials, such as wurtzite AlN and wurtzite GaN [13]. Thus, it is crucial to enhance the out-of-plane electromechanical effects for application advancements of 2D TMDs.

A widely used method to enhance electromechanical coupling effects is to break the inversion symmetry [14, 15]. Density functional theory (DFT) simulations revealed that multilayer Janus TMDs with mirror-asymmetric crystal structures have much larger out-of-plane piezoelectric coefficients that are comparable and even larger than those of AlN and GaN [9, 13]. However, it might be challenging to precisely control the reflection asymmetry for each layer. Another approach for the structural-symmetry breaking is to introduce vacancies into TMDs. For instance, an enhanced out-of-plane piezoresponse can be observed in 2D hexagonal $MoTe_2$ (2H-$MoTe_2$) due to the formation of Te vacancies through thermal annealing [14]. Nevertheless, it might be hard to control the annealing process, which is likely to cause degenerative doping of vacancies, damaging the electronic and optical properties [16]. Recently, it has been found that heterostructure interfaces can induce polar structures in semiconductors regardless of structure symmetry, resulting in emergent piezoelectric effects [17], which provides another novel method to enhance the out-of-plane electromechanical effects.

2D materials can easily be vertically stacked by vdW forces with a large number of combinations to form countless 2D heterostructures, greatly extending the range of functionalities of the 2D material family [5]. 2D heterostructures can be directly grown by chemical vapor deposition (CVD) or physical epitaxy, or obtained by mechanically stacking 2D layers [1, 5]. It has been well demonstrated that pristine 2H-MoS_2 has only a small out-of-plane piezoelectric coefficient d_{33}^{eff} originating from flexoelectricity [8]. In this work, taking 2H-MoS_2 nanoflakes as a typical example of 2D TMD materials, we demonstrate a facile approach to break the out-of-plane structural symmetry of 2D TMDs and increase their out-of-plane electromechanical behaviors by heterostructure engineering. 2D hexagonal boron nitride (h-BN) possesses high chemical stability, excellent resistance to mechanical manipulation, a large bandgap of ~ 6 eV, a high dielectric constant, superior optical transparency, and no dangling bonds and charge traps. These merits enable 2D h-BN to serve as an ideal encapsulating or interface layer or substrate for 2D materials-stacked devices, improving their optical properties, electrical and optoelectronic performances, and device stability [18, 19]. Thus, h-BN is a suitable candidate for breaking the reflection symmetry of TMDs through forming heterostructures. We built MoS_2/BN heterostructures by stacking a monolayer of h-BN on 2H-MoS_2 nanoflakes. The electromechanical performances were studied by piezoresponse force microscopy (PFM). PFM is a powerful atomic force microscopy (AFM) based technique that can measure the electromechanical deformation resulting from the converse piezoelectric or/and converse flexoelectricity in materials under an applied electric field. Due to the breaking of the mirror symmetry, the MoS_2/BN heterostructures exhibited much stronger out-of-plane electromechanical effects than pristine MoS_2 nanoflakes. Kelvin probe force microscopy (KPFM) is also an AFM based technique that can map the surface potential distribution of a wide range of nanostructures. It has been used to locate the work function in materials [20]. We further used KPFM to investigate the surface potential change in the samples to identify the existence of dipoles at the heterostructure interface. The interface polar structure on the MoS_2 surface plays a significant role in the enhancement of the out-of-plane piezoresponse.

2 Results and discussion

2.1 Morphology characterization and electromechanical testing method

Figure 1(a) shows an optical microscopy image of an individual as-prepared 2H-MoS_2 nanoflake with its corresponding contact-mode AFM image shown in Fig. 1(b). After obtaining the MoS_2 nanoflakes on substrates, we transferred monolayer h-BN onto the MoS_2 nanoflakes to form MoS_2/BN heterostructures (see Methods). The optical microscopy image (Fig. 1(c)) shows two MoS_2 nanoflakes covered by monolayer h-BN. Figure 1(d) shows another individual BN-covered MoS_2 nanoflake. From its corresponding AFM image (Fig. 1(e)), we can observe that the nanoflake is partially coated by BN, indicating the successful fabrication of the MoS_2/BN heterostructure. Figure 1(f) schematically illustrates the configuration of PFM measurements on the fabricated MoS_2/BN heterostructures. The Au layer coating on the Si/SiO_2 substrate serves as the bottom electrode, which can minimize electrostatic effects on the PFM signals. The MoS_2 nanoflake covered by the monolayer h-BN is situated on the Au layer. Alternating current (AC) voltages with a specific frequency of 60 kHz are applied across the heterostructure by a conductive AFM tip contacting to the surface of the sample. Due to the converse electromechanical coupling effects of samples, the AC voltage induces a mechanical deformation which is detected by a position sensitive photodiode. The resulting signal is read out by a lock-in amplifier.

2.2 Out-of-plane electromechanical performance of MoS_2

The out-of-plane PFM results of pristine MoS_2 nanoflakes are shown in Fig. 2. Figure 2(a) shows an AFM topography image of an individual MoS_2 nanoflake taken during the PFM scanning under no bias. The height profile along the line in Fig. 2(a) indicates that the nanoflake has a thickness of approximately 60.4 nm (Fig. 2(b)). In all PFM measurements, the drive frequency was set to be 60 kHz, which is far from the contact resonance frequency (~ 350 kHz) of the tip-sample system. Figure S1 in the Electronic Supplementary Material (ESM) shows the determination of the frequency of the AC voltage for the PFM measurements. This should ensure that no obvious topographic artifacts would be caused by tip motion during scanning [8]. Figure 2(c) shows that without an AC voltage applied, there is no obvious contrast between the MoS_2 and Au in the piezoresponse amplitude image of the framed area in Fig. 2(a) since no electromechanical displacement in the nanosheet was generated without an external electric field. The absence of contrast also

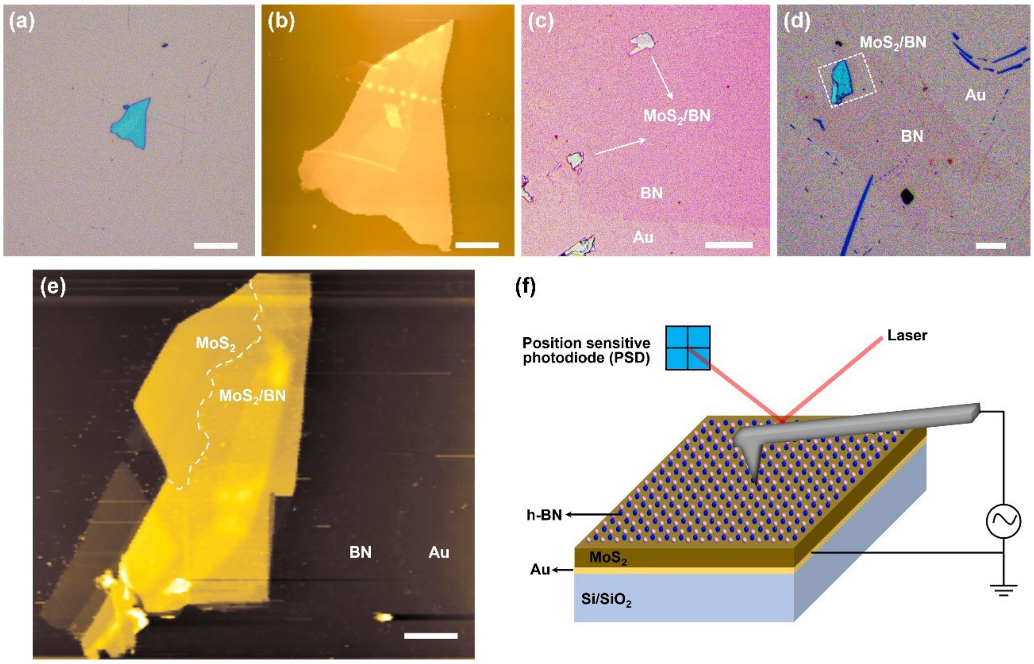

Figure 1 Morphology characterization and configuration of PFM measurements. (a) Optical microscopy image and (b) the corresponding contact-mode AFM topography image of an individual MoS_2 nanoflake. (c) Optical microscopy image of MoS_2/BN heterostructures. (d) Optical microscopy image and (e) the corresponding contact-mode AFM image of an individual MoS_2/BN sample. (f) Schematic showing the configuration of the PFM measurement on the MoS_2/BN heterostructure located on an Au-coated Si/SiO_2 substrate. Scale bars, 50 μm in (a) and (d), 10 μm in (b) and (e), 100 μm in (c).

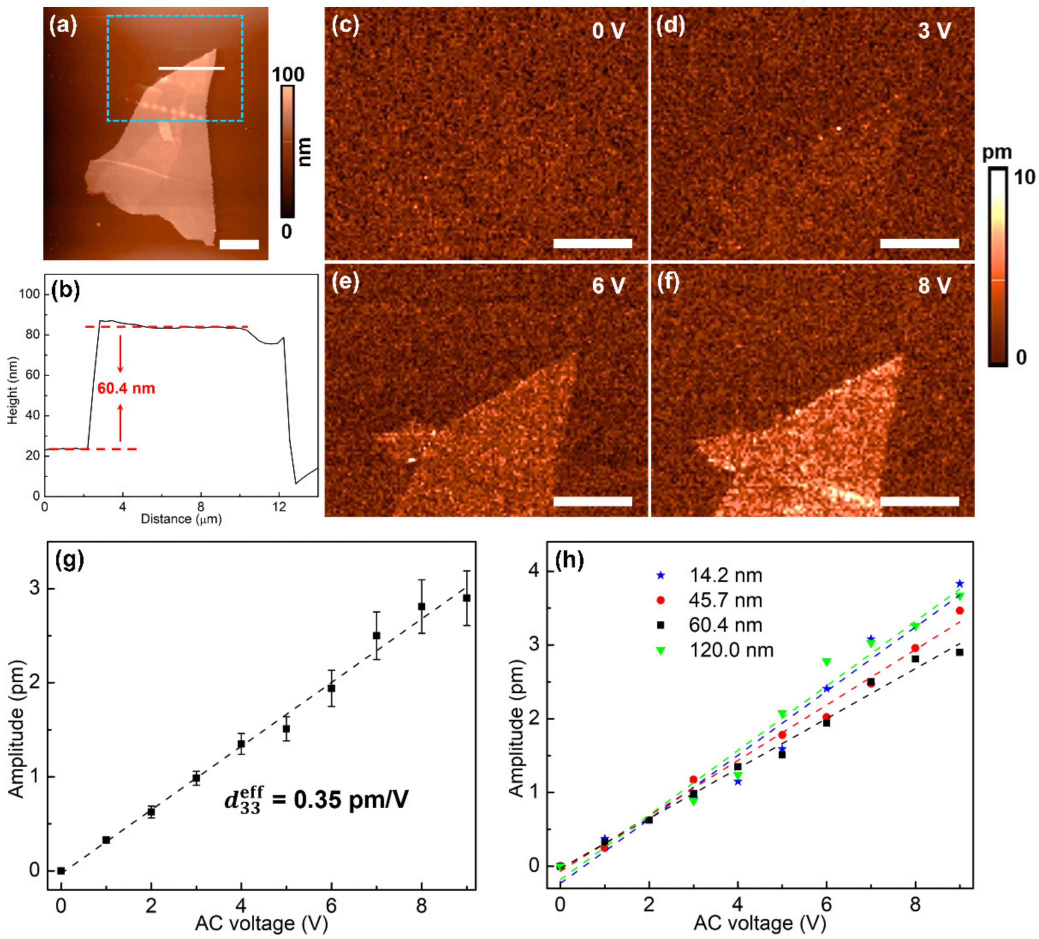

Figure 2 PFM amplitude results of an individual MoS_2 nanoflake with a thickness of 60.4 nm. (a) Contact-mode AFM image of the nanoflake. (b) Height profile along the line in panel (a). (c)–(f) PFM amplitude images of the framed area in panel (a) measured under AC voltages of 0, 3, 6, and 8 V, respectively. (g) and (h) PFM amplitudes as a function of the applied AC voltage for the MoS_2 nanoflake shown in (a), and for MoS_2 nanoflakes with varying thicknesses, respectively. Scale bars, 10 μm.

confirms that any effects on the piezoresponse signal brought by crosstalk of the surface topography are negligible. With the AC voltage increased to 3 V, the contrast between MoS_2 and Au emerged (Fig. 2(d)), indicating the occurrence of the mechanical deformation in MoS_2 caused by the external electric field. Continued increases in the drive voltage result in stronger piezoresponses, as suggested by the gradually enhanced contrasts (Figs. 2(d)–2(f)). From the AFM topography images of the nanoflake before and after the PFM tests, we can see that no mechanical damage of the sample is caused (Fig. S2 in the ESM).

Besides the topographic artifacts, the electrostatic force between the AFM tip and the Au film may also influence the piezoresponse signal [8, 21], as discussed in Note S1 and Fig. S3 in the ESM. To clarify that the electrostatic force plays a minimal role in the piezoresponse signal, we carried out PFM tests for a MoS_2 nanoflake by applying various direct current (DC) voltages with a constant AC voltage of 6 V, as shown in Fig. S3 in the ESM. The piezoresponse amplitudes are found to be nearly the same under different DC voltages, suggesting that the effects brought by the electrostatic force can be neglected. Another electromechanical effect that is likely to cause mechanical deformation is electrostriction. However, it cannot contribute to the PFM signal since the electrostrictive strain is proportional to the square of the applied electric field while the piezoresponse is detected as the first harmonic of the tip deflection, as illustrated in Note S2 in the ESM. It has been widely reported that bulk 2H-MoS_2 possesses no out-of-plane piezoelectricity due to its D_{3h} crystal structure which is centrosymmetric [22]. Piezoelectricity only exists in MoS_2 when its thickness decreases to a monolayer or to a limited odd number of layers due to the breaking of the inversion symmetry. In this case, however, there are only non-zero components for the in-plane piezoelectricity in the piezoelectric tensor. With only one piezoelectric coefficient d_{11}, the piezoelectricity of monolayer MoS_2 can be fully described [8, 22]. The absence of out-of-plane piezoelectric coefficients indicates that piezoelectricity cannot account for the observed electromechanical responses in the as-prepared MoS_2 nanoflakes, which must therefore be due to flexoelectricity [8].

To quantify the out-of-plane mechanical deformation of a material subject to an electric field, we need to calculate the effective piezoelectric coefficient, which is given by $d_{33}^{\mathrm{eff}} = \Delta u / V_{\mathrm{AC}}$, where Δu is the tip vertical deflection, and V_{AC} is the applied AC voltage on the tip. Since a noise signal can be detected from the Au during the PFM measurements even under no applied voltage, which can be superimposed onto the true piezoresponse signal from the MoS_2 nanoflakes, a background subtraction method should be adopted to determine the true value of Δu, as illustrated in Fig. S4 and Note S3 in the ESM [8]. We plotted the curve of the piezoresponse amplitude as a function of the applied voltage, as shown in Fig. 2(g), from which we can observe that the amplitude increases linearly with the AC voltage. Figure 2(g) suggests that d_{33}^{eff} of MoS_2 is independent of the applied voltage. The value of d_{33}^{eff} calculated to be 0.35 pm/V from the linear fit of the curve in Fig. 2(g). We further conducted PFM tests on MoS_2 nanoflakes with different thicknesses. As shown in Fig. 2(h), there is a linear relationship between the PFM amplitude and the AC voltage for all the samples. The d_{33}^{eff} coefficient of the MoS_2 nanoflakes was found to be independent of their thicknesses since the slopes of the fitting curves are close to each other, with the values ranging from 0.35 to 0.44 pm/V. In comparison, monolayer MoS_2 was experimentally measured to have a d_{33}^{eff} of 1.03 pm/V in previous works [8].

2.3 Out-of-plane electromechanical performance of MoS_2/BN

Figure 3 shows the out-of-plane PFM results of the MoS_2/BN heterostructure with a thickness of 218 nm. The PFM amplitude images of the framed area of the MoS_2/BN sample shown in Fig. 3(a) also exhibit gradually enhanced contrast between MoS_2/BN and Au with the increase of the AC voltage, as shown in Figs. 3(b)–3(e). To be noted, the ultra-strong contrast at the edge of the nanoflake was caused by the large step height from the nanoflake to the substrate. We also rule out the contributions from topographic artifacts and electrostatic force to the piezoresponse signals for MoS_2/BN, as shown in Fig. S6 in the ESM. The results indicate that with the increase of the AC voltage, the electromechanical response for the heterostructures is enhanced accordingly. Although the PFM amplitude increases monotonically with the AC voltage increasing, the PFM amplitude–voltage curve of the heterostructure does not exhibit a linear feature, as shown in Fig. 3(f). The PFM amplitude increases slowly below the voltage of 4 V while increases rapidly above 4 V. Together with the information of the piezoresponse phase (Fig. S7 in the ESM), we can also calculate the true vertical deflections for MoS_2/BN using the background subtraction method. The displacement amplitude for the heterostructure reaches ~ 5.5 pm under 9 V, which is much larger than that (2.8–3.8 pm) of the pristine MoS_2 nanoflakes. It is reasonable to ascribe the enhancement of the PFM response to the capping of the monolayer BN on MoS_2 nanoflakes. It is likely due to the symmetry-breaking and the polarization at the MoS_2-BN interface after the formation of heterostructures, which will be demonstrated later.

We further compared the electromechanical behaviors of MoS_2/BN with decreasing thicknesses of 80, 41.2, and 28.9 nm with that of 218 nm. As shown in Fig. 3(g), the piezoresponse amplitudes of these thinner heterostructures also increase slowly below 4 V while soaring above 4 V. In contrast to the pristine MoS_2 nanoflakes, the PFM amplitude–voltage curves of MoS_2/BN show a thickness dependence. Specifically, as the thicknesses of the heterostructures decrease from 218 to 28.9 nm, the PFM amplitude is growing faster when the AC voltage is above 4 V. For AC voltages up to 9 V, the displacement amplitude of MoS_2/BN increases from ~ 5.5 pm to a significant value of ~ 21 pm as the thickness is decreased from 218 to 28.9 nm. Below ~ 4 V, no obvious linear relationship can be observed between the PFM amplitudes and the voltage, while above 4 V, the amplitude shows a linear relationship with the voltage, which is proper to be used to calculate effective piezoelectric coefficients. Thus, we can obtain d_{33}^{eff} of the heterostructures by calculating the slopes of the fitting curves for the linear section, which is 1.03, 2.02, 3.06, and 4.44 pm/V, respectively, with the thickness decreasing as above. More efforts are needed to reveal the underlying mechanisms for the nonlinear feature and the thickness dependence of the PFM amplitude–voltage curves of MoS_2/BN, which will be discussed in the following contents.

In order to better compare the electromechanical performances of MoS_2 and MoS_2/BN, the PFM amplitude–voltage curves of the two kinds of samples are plotted in one figure, as shown in Fig. 3(h). It can be seen that except for the 218 nm-thick MoS_2/BN, the other heterostructures show a great increase in the piezoresponse amplitude compared to the pristine MoS_2 when the AC voltage is above 4 V. In-plane piezoelectricity has been often demonstrated in 2D 2H-TMDs while out-of-plane piezoelectricity has received less

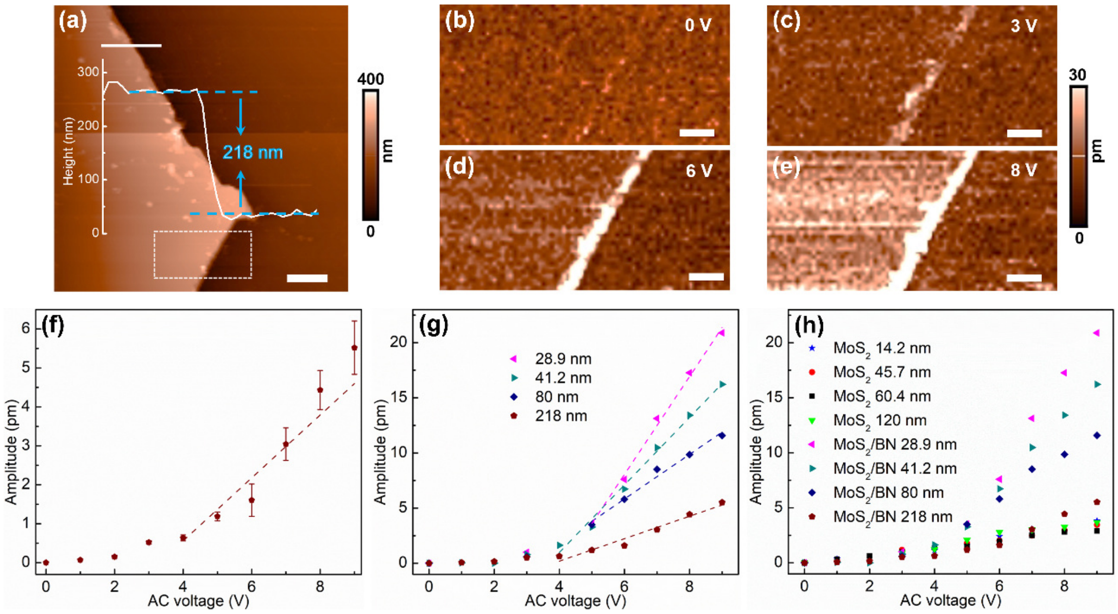

Figure 3 PFM amplitude results of MoS_2/BN heterostructures. (a) Contact-mode AFM image of the heterostructure. Inset is the height profile along the line. (b)–(e) PFM amplitude images of the framed area in (a) measured under AC voltages of 0, 3, 6, and 8 V, respectively. (f) and (g) PFM amplitude as a function of the applied AC voltage for MoS_2/BN shown in (a) and for MoS_2/BN with varying thicknesses, respectively. (h) Comparison of the out-of-plane piezoresponse amplitude between pristine MoS_2 and MoS_2/BN. Scale bars, 5 μm.

attention due to the absence of nonzero out-of-plane piezoelectric coefficients. Even though out-of-plane electromechanical coupling derived from flexoelectricity can be detected in 2D 2H-TMDs, the value of d_{33}^{eff} is generally smaller than that of their in-plane piezoelectric coefficient. For instance, d_{33}^{eff} for monolayer MoS_2 was measured to be 1.03 pm/V by PFM [8]. In comparison, monolayer MoS_2 has a measured d_{11} of 1.85 pm/V and a d_{11} coefficient obtained through computational methods ranging from 2.91 to 3.73 pm/V [22, 23]. The d_{33}^{eff} coefficients for other TMDs, such as WS_2 and WSe_2, were measured to be only 0.71 and 0.43 pm/V, respectively [11], and in this work, d_{33}^{eff} for the tested MoS_2 nanoflakes ranges from 0.35 to 0.44 pm/V. The values of d_{33}^{eff} for TMDs are usually not comparable with those of the commonly used wurtzite bulk piezoelectric materials, such as wurtzite GaN (3.1 pm/V) and wurtzite AlN (5.1 pm/V) [13]. The weak out-of-plane electromechanical response of TMDs limits their applications in nanodevices. Given that the d_{33}^{eff} coefficient of MoS_2/BN in this work is enhanced to 4.44 pm/V, which can rival that of conventional piezoelectric materials, such as GaN and AlN, the results pave a way to help TMDs overcome this limitation. The MoS_2/BN heterostructures may be taken as candidate materials for piezoelectric energy-harvesting devices, nanoelectromechanical systems, and sensors. For instance, it is possible that 2D TMDs heterostructures can replace AlN and it can be grown or exfoliated on desired substrates, applied in surface acoustic wave devices, sensors, and actuators [24].

2.4 Out-of-plane electromechanical performance of monolayer h-BN

Obviously, the enhancement of the electromechanical performances of MoS_2/BN is related to the monolayer h-BN. To clarify that the enhancement of the piezoresponse signal of MoS_2/BN is not solely ascribed to a mechanical deformation of the BN induced by electromechanical effects, we conducted PFM tests on the monolayer h-BN film. Figure 4(b) is the AFM topography image of the framed area in Fig. 4(a) showing a monolayer h-BN film on a gold-covered Si/SiO_2 substrate. The PFM results corresponding to Fig. 4(b) are shown in Figs. 4(c)–4(h). When the AC voltage is not applied, no piezoresponse contrasts (Figs. 4(c) and 4(f)) can be observed. With the AC voltage increased to 6 V, we can discern the piezoresponse contrasts in both the amplitude image (Fig. 4(d)) and its corresponding phase image (Fig. 4(g)), suggesting that there was mechanical deformation induced in BN. The contrasts in the amplitude image (Fig. 4(e)) and its corresponding phase image (Fig. 4(h)) become stronger under an AC voltage of 9 V. Since the piezoresponse phase signals from BN and Au are nearly the same (Fig. S8 in the ESM), the actual piezoresponse amplitudes of the monolayer BN are calculated to be only 0.26 and 0.34 pm for the voltages of 6 and 9 V, respectively, according to the background subtraction method illustrated in Fig. S4 in the ESM. The average value of d_{33}^{eff} for the monolayer h-BN is 0.04 pm/V, which is one order of magnitude smaller than that of MoS_2.

Monolayer h-BN also has a crystal structure belonging to the D_{3h} ($\bar{6}m2$) point group, which is the same with 2H-MoS_2 [22]. The piezoelectric tensor for monolayer h-BN can be written as

$$\begin{bmatrix} e_{11} & -e_{11} & 0 & 0 & 0 & 0 \\ 0 & 0 & 0 & 0 & 0 & -e_{11} \\ 0 & 0 & 0 & 0 & 0 & 0 \end{bmatrix} \tag{1}$$

where no out-of-plane nonzero components exist, indicating that the measured piezoresponse of h-BN does not originate from out-of-plane piezoelectricity. Figure S6 in the ESM shows that the electrostatic force has no effects on the piezoresponse signal from the monolayer h-BN on Au. Since the flexoelectric tensor of monolayer h-BN has nonzero components in the out-of-plane direction, the piezoresponse should result from the out-of-plane flexoelectricity. For the ultrathin monolayer h-BN, its effective converse flexoelectric coefficient accounting for the out-of-plane deformation, μ_{eff}, can be given by

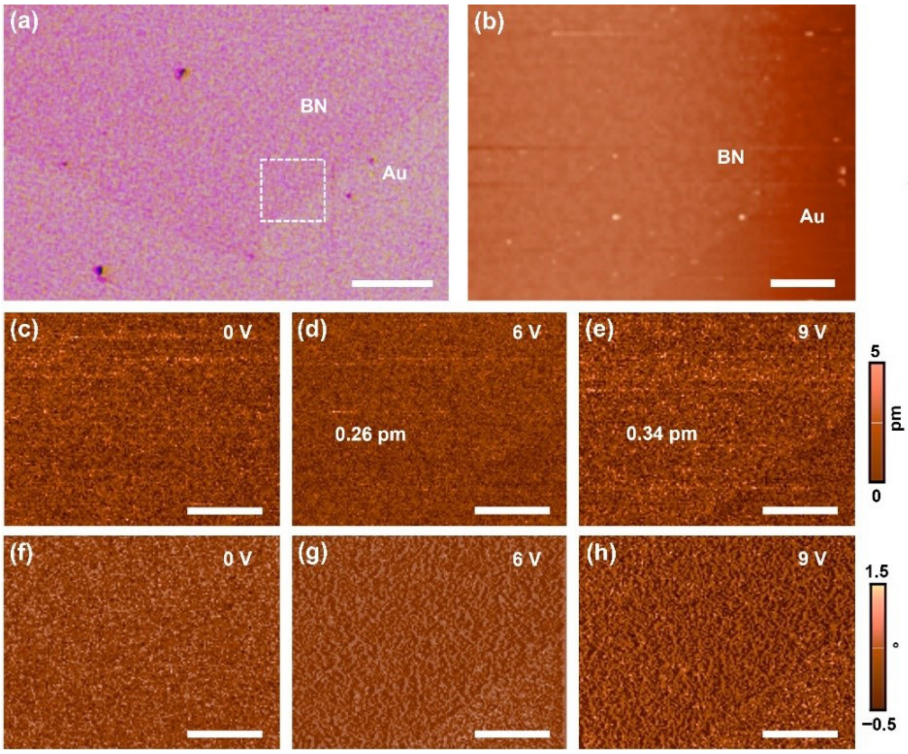

Figure 4 Morphology characterization and PFM results of the monolayer h-BN. (a) Optical microscopy image of the monolayer BN. (b) AFM topography image of the framed area in panel (a). (c)–(e) PFM amplitude images under AC voltages of 0, 6, and 9 V, respectively. (f)–(h) PFM phase images corresponding to (c)–(e), respectively. Scale bars, 50 μm in (a), 5 μm in (b), 10 μm in (c)–(h).

$$\mu_{\mathrm{eff}} = \frac{d_{33}^{\mathrm{eff}} Yt}{2} \tag{2}$$

where Y is Young's modulus, and t is the thickness of monolayer h-BN, respectively. By taking Y as 865 GPa and t as 0.42 nm [25], the value of μ_{eff} is estimated to be ~ 0.00083 nC/m, which is of the same order of magnitude with that (0.00026 nC/m) obtained by computational methods and is much smaller than that (0.032 nC/m) of monolayer MoS_2 [26]. It should be the ultrasmall out-of-plane flexoelectric coefficient that leads to the weak piezoresponse signal of the monolayer h-BN. Therefore, the enhanced out-of-plane piezoresponse signal of MoS_2/BN cannot be due to the intrinsic electromechanical effects of the monolayer h-BN.

2.5 Mechanisms of the enhanced electromechanical performance for MoS_2/BN

Efforts have been made to create or enhance the out-of-plane piezoelectricity of 2H-TMDs by breaking the out-of-plane mirror symmetry. A synthetic approach is to grow Janus monolayer TMDs [15]. For instance, Janus monolayers of MoSSe were synthesized by replacing the top-layer S with Se atoms. Since the S–Mo and S–Se bonding lengths are unequal, the out-of-plane reflection symmetry is broken. Out-of-plane piezoelectricity was proven to exist in the MoSSe monolayers by PFM measurements [15]. DFT simulations revealed that multilayer Janus MXY (M = Mo or W, X/Y = S, Se, or Te, and X ≠ Y) TMDs have strong out-of-plane piezoelectricity, with the out-of-plane piezoelectric coefficient d_{33} ranging from 5.7 to 13.5 pm/V depending on the stacking sequence, which is even larger than that (5.6 pm/V) of the widely used piezoelectric wurtzite AlN. The enhanced out-of-plane piezoelectricity is probably due to the dipole–dipole interactions between the vdW gaps [9]. However, the synthetic method for creating symmetry-breaking in the out-of-plane direction involves sophisticated chemical processes. Another strategy to create symmetry-breaking for 2H-TMDs is doping. For instance, Kang et al. introduced Te vacancies in 2H-$MoTe_2$ flakes, leading to strong out-of-plane piezoelectricity due to the atomic-scale symmetry breaking inside 2H-$MoTe_2$ [14]. However, doping in TMDs can hardly be controlled and may result in a loss of their intrinsic properties, such as the loss of semiconducting properties and optoelectronic properties [16]. Thus, it is worth discovering a facile and noninvasive method for the breaking of the out-of-plane mirror symmetry to enhance the out-of-plane electromechanical performances of TMDs. It has been reported that an external electric field may lead to phase transitions in a material from a symmetric structure to an asymmetry structure. In this case, the external field is likely to induce an enhanced out-of-plane piezoresponse. In our work, the linear dependence of the PFM amplitude on the AC voltage shown in Fig. 2 indicates that no such symmetry-breaking in the form of phase transition was generated by AC voltages.

2D vdWs materials can be considered as assemblies, where monolayers are held together by weak vdWs forces. They relieve the stringent requirement for fabricating heterostructures with strong chemical bonding. We can directly fabricate vdWs heterostructures by vertically stacking different layered materials. The fabrication methods for vdWs heterostructures include mechanically-assembled stacks and direct growth by physical epitaxy or CVD [5]. Such vdWs heterostructures give rise to a plethora of exciting physical phenomena, yielding a wide range of applications [5, 27]. One can create the mirror symmetry-breaking in 2H-TMDs by fabricating heterostructures since the stacking of the layers must be disturbed at the interface. Moreover, a band offset can occur at the semiconductor-semiconductor junctions or semiconductor-metal junctions in 2D heterostructures, leading to strong polarizations at the interfaces, which contributes to enhanced piezoelectric properties. Due to these mechanisms, many kinds of heterostructures were found to exhibit largely enhanced out-of-plane piezoelectricity compared to their single constituent parts. For instance, the d_{33}^{eff} coefficients of In_2Se_3/MoS_2 and In_2Se_3/p-Si heterostructures could reach approximately 17.5 and 9.19 pm/V, respectively, compared to that (~ 7.6 pm/V) of pristine In_2Se_3 nanoflakes [28–30]. Even though these values are larger than that of MoS_2/BN in this work, monolayer BN can endow MoS_2/BN other merits. For example, monolayer BN can preserve the best of the optical properties of MoS_2 and protect MoS_2 from degradation [18]. Also formed by TMDs without intrinsic out-of-plane piezoelectricity, the SnS_2/SnS heterostructure was found to have an enhanced d_{33}^{eff} coefficient (~ 4.75 pm/V) than that (~ 3.37 pm/V) of SnS_2 and that (~ 1.85 pm/V) of SnS [31]. The out-of-plane piezoelectricity of MoS_2/BN heterostructures is comparable to that of the SnS_2/SnS heterostructure. In addition to the breaking of the mirror symmetry, more mechanisms may account for the large out-of-plane piezoelectricity of MoS_2/BN, as revealed later.

To further explore the roles of the monolayer h-BN of MoS_2/BN on the enhanced out-of-plane piezoresponse, we carried out KPFM measurements on pristine MoS_2 nanoflakes, monolayer h-BN films, and MoS_2/BN heterostructures. KPFM can be used to measure the surface potential (V_{sp}) of samples, which is described as

$$V_{sp} = \frac{\varphi_S - \varphi_{tip}}{e} \tag{3}$$

where φ_S and φ_{tip} are the work functions of the sample and the AFM tip used, respectively, and e is the electronic charge. During the KPFM tests, the bottom surfaces of the materials are grounded while φ_{tip} is constant. Thus, it is expected that different V_{sp} values will be obtained due to the work function change in different samples.

Figure 5 shows the KPFM results of MoS_2, BN, and MoS_2/BN. To be noted, since it is the surface potential change in the samples that is the key point to be discussed, the work function of the conductive tip was not calibrated during the KPFM measurements. Therefore, the surface potentials obtained for the three kinds of samples here are not their true values. The surface potential of the Au layer coated on the Si/SiO_2 substrate is close to zero due to the similar work function of the Au layer and the conductive AFM tip. Thus, the values of the surface potential for different samples are calculated with the Au layer as reference so that the surface potential of different samples can be compared with each other. Figures 5(b) and 5(e) show the surface potential maps of the pristine MoS_2 on Au and the monolayer BN on Au, respectively. According to their corresponding statistical distribution of the surface potentials (Figs. 5(c) and 5(f)), it is found that the pristine MoS_2 on Au and the monolayer BN on Au have average values of −12.1 and 21.6 mV, respectively. In comparison, the surface potential of the MoS_2/BN heterostructure on Au is −84.5 mV, which has a difference of 72.4 mV with that of the pristine MoS_2.

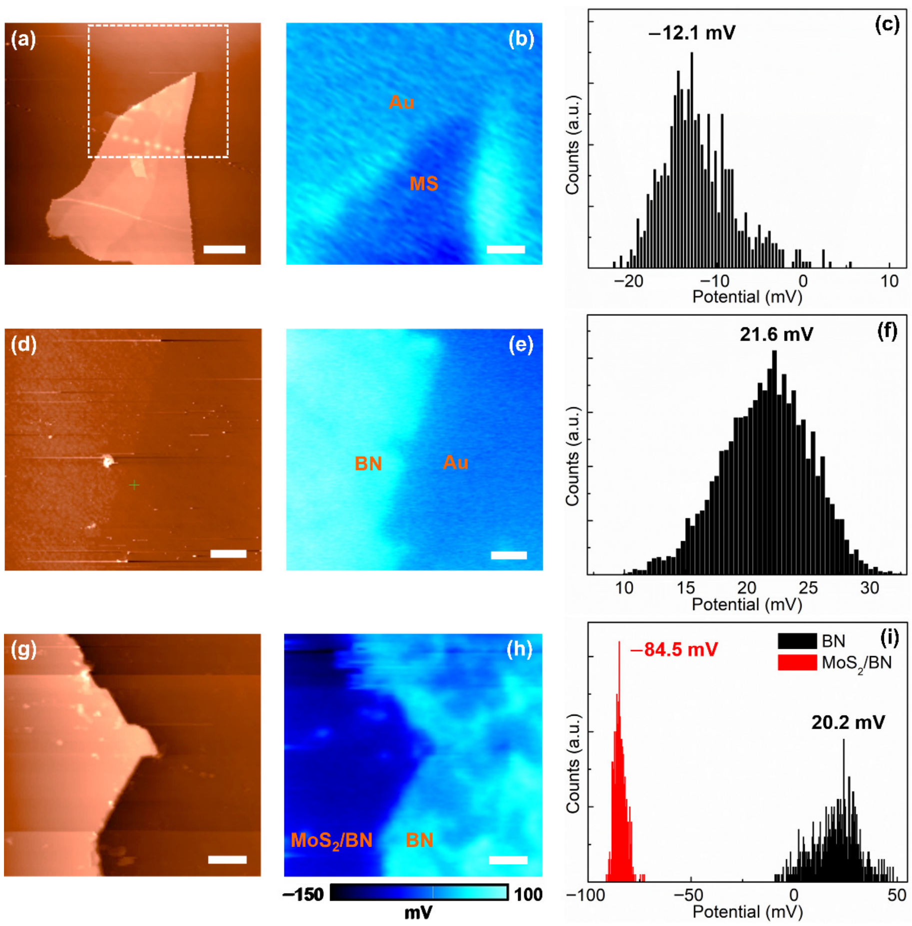

Figure 5 KPFM mapping results of the surface potential. (a) AFM topography image, (b) the corresponding surface potential map, and (c) the histogram of the surface potential of MoS_2, respectively. (d) AFM topography image, (e) the corresponding surface potential map, and (f) the histogram of the surface potential of monolayer h-BN, respectively. (g) AFM topography image, (h) the corresponding surface potential map, and (i) the histogram of the surface potential of MoS_2/BN, respectively. Scale bars, 10 μm in (a), (d), and (e), 5 μm in (b), (g), and (h).

Although this difference in the surface potential might not be accurate due to the influences from the Au substrate and the absorbates on the surfaces of the samples [32, 33], it could be evidence that the effective work function in MoS_2/BN was increased. Calculation results based on DFT in a previous work indicated that there is no obvious charge exchange between BN and MoS_2. Thus, the increase of the effective work function of MoS_2/BN is most likely caused by the lattice strain induced inside the heterostructure [34]. The preexisting lattice strain near the interface can form a polar structure. Moreover, due to the existence of sulfur vacancies in the surface of MoS_2, charges are likely trapped at the interface with BN, forming dipoles [35–37]. The polar structure at the interface can contribute to the out-of-plane electromechanical performances of MoS_2/BN.

We further conducted molecular dynamic (MD) simulations for the out-of-plane piezoelectric behaviors of monolayer-MoS_2/monolayer-BN. The computational details and results can be seen in Note S5, Fig. S9, and Tables S1 and S2 in the ESM. Even though the size of the simulated heterostructure here is not comparable to those in our experiments, the simulation results are still helpful to reveal the mechanisms for the enhancement of the out-of-plane electromechanical properties. Figures 6(a) and 6(b) show the optimized structure of the monolayer-MoS_2/monolayer-BN heterostructure. The average lattice constant, a, of the optimized heterostructure is examined to be 12.564 Å in comparison with that (12.732 Å) of a 4 × 4 supercell of pristine MoS_2 and that (12.510 Å) of a 5 × 5 supercell of pristine h-BN, respectively. Thus, lattice strains induced in the a direction for MoS_2 and BN are ~ 1.32% and 0.43%, respectively. Such lattice strain is likely to create a polar structure near the interface [38], contributing to the electromechanical properties [39, 40].

Figure 6(c) shows that the piezoelectric polarization of monolayer-MoS_2/monolayer-BN increases linearly with the applied stress. The piezoelectric coefficient d_{33}^{eff} of monolayer-MoS_2/monolayer-BN is calculated to be ~ 1.82 pm/V. Figure 6(d) shows the flexoelectric behavior with a linear feature of the monolayer-MoS_2/monolayer-BN heterostructure. The flexoelectric coefficient mainly contributing to the out-of-plane polarization, μ_{48}, is calculated to be ~ 0.0516 nC/m. According to the Eq. (2) (thickness and Young's modulus of MoS_2/BN displayed in Table S1 in the ESM), the effective out-of-plane piezoelectric coefficient induced by μ_{48} is estimated to be ~ 0.24 pm/V. Thus, the total d_{33}^{eff} coefficient is ~ 2.06 pm/V when including both of the piezoelectric polarization and flexoelectric polarization. The value is much larger than the d_{33}^{eff} coefficient (1.03 pm/V) of monolayer MoS_2 but smaller than those of the thinner heterostructures obtained in our experiments [8]. This variation is probably due to the extremely small size of the used MoS_2/BN model and the absence of sulfur vacancies in the simulated MoS_2.

A phenomenological theory based on the built-in effect in Schottky junctions and the electrostriction effect has been established by Yang et al. to reveal the microscopic mechanism of the interface piezoelectric effects in semiconductors [17]. Narvaez et al. reported a barrier-layer mechanism based on surface piezoelectricity to explain the large effective flexoelectric coefficient in oxide semiconductors [39]. However, the semiconductors were doped with transitional metals in their works. The enhanced out-of-plane piezoresponse of MoS_2/BN should not be due to the polar structures in the Schottky junctions of MoS_2 or MoS_2/BN with metal electrodes. This can be verified by the fact that the piezoresponse of pristine MoS_2 is not enhanced. In this work, since the polar structure in MoS_2/BN is located at the surface of the MoS_2, it is similar to a spontaneously polarized surface layer in a ferroelectric ceramic. The outmost surface polar layer is equivalent to a piezoelectric thin film [40], leading to a strong out-of-plane electromechanical response. According to the piezoelectric-composite model [40, 41], the MoS_2/BN heterostructure can be treated as a composite consisting of a piezoelectric surface layer and a nonpiezoelectric bulk body, as illustrated in Note S5 and Fig. S10 in the ESM. The d_{33}^{eff} coefficient can be described as

$$d_{33}^{\text{eff}} \approx d_{33}^{\text{S}} \frac{\varepsilon_2 h_1}{\varepsilon_1 h_2} \tag{4}$$

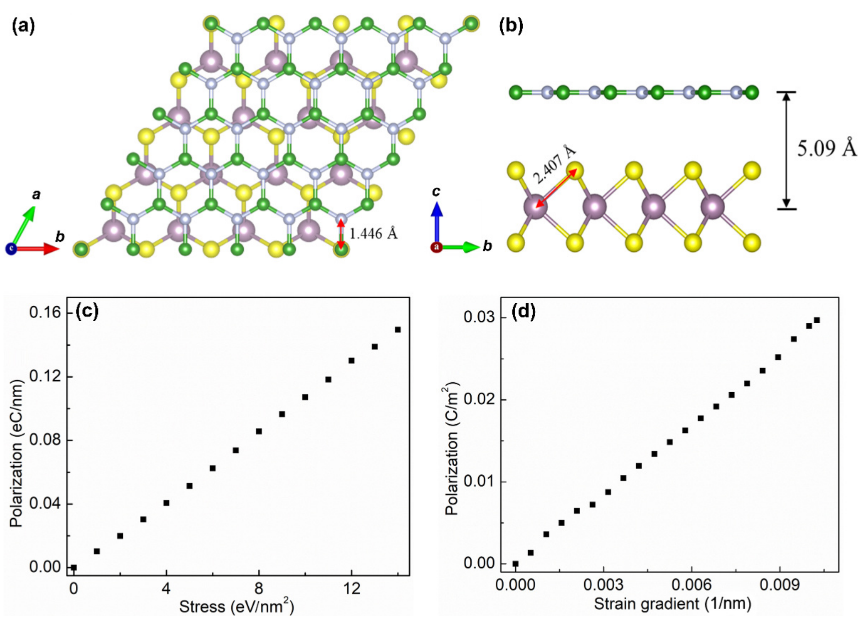

Figure 6 Computational results. (a) Top-view and (b) side-view of a schematic monolayer-MoS_2/monolayer-BN heterostructure with 1.4% lattice mismatch. Purple, yellow, green, and light blue balls represent Mo, S, B, and N atoms, respectively. The red arrow in (a) marks the bond length of B–N and Mo–S. The average distance from Mo atoms to the BN sheet is 5.09 Å. (c) Piezoelectric behavior and (d) flexoelectric behavior of the heterostructure, respectively.

where ε_1 and ε_2 are the dielectric constants of the surface layer and the bulk, respectively, and h_1 and h_2 are the thicknesses of the surface layer and the bulk, respectively [40, 41].

We then look back on the thickness dependence of the PFM amplitude–voltage curves for MoS_2/BN shown in Fig. 3(g). According to Eq. (4), the d_{33}^{eff} coefficient of MoS_2/BN is inversely proportional to the thickness of the MoS_2 bulk, which is in agreement with the results in Fig. 3(g). The nonlinear behavior of the piezoresponse for MoS_2/BN shown in Fig. 3 is most likely due to the asymmetry created by the build-in fields at the junction of MoS_2 with the Au substrate and that of MoS_2/BN with the Au-coated AFM tip [42]. As shown by the KPFM results in Fig. 5, the capping of BN on MoS_2 leads to the increase of the effective work function of MoS_2. This indicates that the height of the potential barrier near the interface between MoS_2 and the Au substrate is different from that of the potential barrier near the interface between MoS_2/BN and the AFM tip. Even though linearly increasing AC voltages was applied, this kind of potential barrier difference can make the effective voltage drop (denoted as V_{eff}) across the MoS_2/BN heterostructure behave nonlinearly [42]. In this work, V_{eff} should have two differentiated regions: V_{eff} shows no linearity below ~ 4 V; above ~ 4 V, V_{eff} equals to V_{AC} and increases linearly. According to the equation describing the relationship between the piezoresponse signal and AC voltages, $A_{PFM} = d_{33}V_{eff}$, where A_{PFM} is the PFM piezoresponse signal, the nonlinearly increasing V_{eff} leads to a nonlinear increase in PFM amplitude [42].

3 Conclusions

In summary, we have shown a facile method to break the out-of-plane structural symmetry of 2D 2H-MoS_2 by heterostructure engineering with monolayer h-BN stacking on MoS_2 nanoflakes. We used PFM to study the electromechanical performances of the as-prepared samples. Due to the breaking of the mirror symmetry, the MoS_2/BN heterostructures exhibit strong out-of-plane electromechanical responses which are much larger than that of pristine MoS_2 when under an AC voltage above 4 V. The effective out-of-plane piezoelectric coefficient d_{33}^{eff} of MoS_2/BN can be enhanced to 4.44 pm/V with the thickness of the heterostructures decreasing, which rivals that of the commonly used bulk piezoelectric material, such as AlN and GaN. Moreover, we carried out KPFM tests on the samples to measure their surface potential. The surface potential change suggests the increase of the effective work function for MoS_2/BN, indicating the formation of a polar structure at the MoS_2/BN interface, which plays a key role in the enhanced out-of-plane piezoresponse. This study offers this material family with broader application potential by utilizing out-of-plane electromechanical effects, such as nanoelectromechanical systems, energy harvesting, and sensors.

4 Methods

4.1 Sample fabrication

High-quality (purity > 99.995%) bulk MoS_2 crystals (2H phase) and monolayer h-BN grown on Si/SiO_2 wafer were purchased from HQ Graphene Inc., Netherlands and Grolltex, America, respectively. Si wafers were cut into small pieces (1 cm × 1 cm) followed by a gold coating process using a gold sputter (JEOL JFC-1300, Japan). MoS_2 nanoflakes were obtained by exfoliating a MoS_2 crystal several times using scotch tapes. The scotch tapes with MoS_2 nanoflakes were pressed onto a homemade polydimethylsiloxane (PDMS) stamp, then were gently removed, leaving MoS_2 nanoflakes on the PDMS stamp. In a similar way, the PDMS stamp with MoS_2 nanoflakes was pressed on the Au-coated Si/SiO_2 substrates and gently removed to finish the transferring.

To fabricate MoS_2/BN heterostructures, a wet transfer method was adopted. In detail, a layer of polymethyl methacrylate (PMMA) was spin-coated on the monolayer h-BN grown on Si/SiO_2 substrates with a speed of 2500 rpm, followed by drying at 110 °C on a hot plate for 0.5 h. The PMMA covered Si/SiO_2/BN sample was then placed in a 1 M NaOH solution at 50 °C to etch away the SiO_2 until the PMMA/BN film was detached from the substrate and floated in the solution. After rinsing with deionized water several times, the PMMA/BN film was picked up by a gold-coated Si substrate with MoS_2 nanoflakes, followed by immersing it in acetone at 80 °C for 2 h and subsequently at 100 °C for 3 min on a hot plate, and finally in isopropanol for 0.5 h.

4.2 Characterization

The morphology was characterized using an optical microscopy (Leica DM1750 M, Germany) and an AFM (NTEGRA Prima, NT-MDT Co., Russia). PFM and KPFM measurements were performed in a contact mode and noncontact mode on the NTEGRA Prima scanning probe microscope in ambient, respectively, using a conductive Cr/Au coated silicon probe (HQ:NSC18/Cr-Au, μMasch) with a spring constant of ~ 2.8 N/m and a free resonance frequency of ~ 75 kHz. AC driven voltages with a frequency of 60 kHz were applied during PFM tests.

4.3 Computational details

The details of MD simulations and DFT calculations were illustrated in Note S4 in the ESM.

Electronic Supplementary Material: Supplementary materials (determination of AC voltage frequency for PFM tests, AFM topography images, ruling out influences from electrostatic force, ruling out the contribution from electrostriction to the piezoresponse, calculation of true vertical deflection, background subtraction for calculating piezoresponse displacements, PFM phase results of MoS_2, PFM amplitude results of MoS_2/BN, PFM phase results of MoS_2/BN, PFM phase results of h-BN, computational details and results, effective piezoelectric coefficient of a piezoelectric composite, and schematic of surface-layer/bulk model) is available in the online version of this article at https://doi.org/10.26599/NR.2025.94907050.

Data availability

All data needed to support the conclusions in the paper are presented in the manuscript and the Electronic Supplementary Material. Additional data related to this paper may be requested from the corresponding author upon request.

Acknowledgements

The authors would like to thank Dr. Brahmanandam Javvaji for the insightful discussion and support.

Declaration of competing interest

All the contributing authors report no conflict of interests in this work.

Author contribution statement

Q. L.: Data curation, investigation, writing manuscript, experimental design. V. K. C.: Data curation, visualization. J. E M.: Writing – review & editing. T. R.: Validation. X. N. J.: Validation. X. Y. Z.: Project administration, funding acquisition. All the authors have approved the final manuscript.

Use of AI statement

None.

References

[1] Han, S. A.; Kim, T. H.; Kim, S. K.; Lee, K. H.; Park, H. J.; Lee, J. H.; Kim, S. W. Point-defect-passivated MoS_2 nanosheet-based high performance piezoelectric nanogenerator. *Adv. Mater.* **2018**, *30*, 1800342.

[2] Meng, C.; Thrane, P. C. V.; Ding, F.; Gjessing, J.; Thomaschewski, M.; Wu, C.; Dirdal, C.; Bozhevolnyi, S. I. Dynamic piezoelectric MEMS-based optical metasurfaces. *Sci. Adv.* **2021**, *7*, eabg5639.

[3] Shi, Y.; Askounis, E.; Plamthottam, R.; Libby, T.; Peng, Z. H.; Youssef, K.; Pu, J. H.; Pelrine, R.; Pei, Q. B. A processable, high-performance dielectric elastomer and multilayering process. *Science* **2022**, *377*, 228–232.

[4] He, Q. Q.; Zeng, Y. S.; Jiang, L. M.; Wang, Z. Y.; Lu, G. X.; Kang, H. C.; Li, P.; Bethers, B.; Feng, S. W.; Sun, L. Z. et al. Growing recyclable and healable piezoelectric composites in 3D printed bioinspired structure for protective wearable sensor. *Nat. Commun.* **2023**, *14*, 6477.

[5] Novoselov, K. S.; Mishchenko, A.; Carvalho, A.; Castro Neto, A. H. 2D materials and van der Waals heterostructures. *Science* **2016**, *353*, eaac9439.

[6] Jiang, J.; Chen, Z. Z.; Hu, Y.; Xiang, Y.; Zhang, L. F.; Wang, Y. P.; Wang, G. C.; Shi, J. Flexo-photovoltaic effect in MoS_2. *Nat. Nanotechnol.* **2021**, *16*, 894–901.

[7] Li, Y. H.; Wang, X.; Tang, D. Q.; Wang, X.; Watanabe, K.; Taniguchi, T.; Gamelin, D. R.; Cobden, D. H.; Yankowitz, M.; Xu, X. D. et al. Unraveling strain gradient induced electromechanical coupling in twisted double bilayer graphene moiré superlattices. *Adv. Mater.* **2021**, *33*, 2105879.

[8] Brennan, C. J.; Ghosh, R.; Koul, K.; Banerjee, S. K.; Lu, N. S.; Yu, E. T. Out-of-plane electromechanical response of monolayer molybdenum disulfide measured by piezoresponse force microscopy. *Nano Lett.* **2017**, *17*, 5464–5471.

[9] Dong, L.; Lou, J.; Shenoy, V. B. Large in-plane and vertical piezoelectricity in Janus transition metal dichalchogenides. *ACS Nano* **2017**, *11*, 8242–8248.

[10] Abdollahi, A.; Domingo, N.; Arias, I.; Catalan, G. Converse flexoelectricity yields large piezoresponse force microscopy signals in non-piezoelectric materials. *Nat. Commun.* **2019**, *10*, 1266.

[11] Brennan, C. J.; Koul, K.; Lu, N. S.; Yu, E. T. Out-of-plane electromechanical coupling in transition metal dichalcogenides. *Appl. Phys. Lett.* **2020**, *116*, 053101.

[12] Huang, S. J.; Qi, L.; Huang, W. B.; Shu, L. L.; Zhou, S. J.; Jiang, X. N. Flexoelectricity in dielectrics: Materials, structures and characterizations. *J. Adv. Dielectr.* **2018**, *8*, 1830002.

[13] Lueng, C. M.; Chan, H. L. W.; Surya, C.; Choy, C. L. Piezoelectric coefficient of aluminum nitride and gallium nitride. *J. Appl. Phys.* **2000**, *88*, 5360–5363.

[14] Kang, S.; Kim, S.; Jeon, S.; Jang, W. S.; Seol, D.; Kim, Y. M.; Lee, J.; Yang, H.; Kim, Y. Atomic-scale symmetry breaking for out-of-plane piezoelectricity in two-dimensional transition metal dichalcogenides. *Nano Energy* **2019**, *58*, 57–62.

[15] Lu, A. Y.; Zhu, H. Y.; Xiao, J.; Chuu, C. P.; Han, Y. M.; Chiu, M. H.; Cheng, C. C.; Yang, C. W.; Wei, K. H.; Yang, Y. M. et al. Janus monolayers of transition metal dichalcogenides. *Nat. Nanotechnol.* **2017**, *12*, 744–749.

[16] Gao, J.; Kim, Y. D.; Liang, L. B.; Idrobo, J. C.; Chow, P.; Tan, J. W.; Li, B. C.; Li, L.; Sumpter, B. G.; Lu, T. M. et al. Transition-metal substitution doping in synthetic atomically thin semiconductors. *Adv. Mater.* **2016**, *28*, 9735–9743.

[17] Yang, M. M.; Luo, Z. D.; Mi, Z.; Zhao, J. J.; E, S. P.; Alexe, M. Piezoelectric and pyroelectric effects induced by interface polar symmetry. *Nature* **2020**, *584*, 377–381.

[18] Zhang, J.; Tan, B. Y.; Zhang, X.; Gao, F.; Hu, Y. X.; Wang, L. F.; Duan, X. M.; Yang, Z. H.; Hu, P. G. Atomically thin hexagonal boron nitride and its heterostructures. *Adv. Mater.* **2021**, *33*, 2000769.

[19] Behura, S.; Nguyen, P.; Che, S. W.; Debbarma, R.; Berry, V. Large-area, transfer-free, oxide-assisted synthesis of hexagonal boron nitride films and their heterostructures with MoS_2 and WS_2. *J. Am. Chem. Soc.* **2015**, *137*, 13060–13065.

[20] Wang, W.; Zhou, L. J.; Hu, S.; Novoselov, K. S.; Cao, Y. Visualizing piezoelectricity on 2D crystals nanobubbles. *Adv. Funct. Mater.* **2021**, *31*, 2005053.

[21] Kalinin, S. V.; Bonnell, D. A. Imaging mechanism of piezoresponse force microscopy of ferroelectric surfaces. *Phys. Rev. B* **2002**, *65*, 125408.

[22] Duerloo, K. A. N.; Ong, M. T.; Reed, E. J. Intrinsic piezoelectricity in two-dimensional materials. *J. Phys. Chem. Lett.* **2012**, *3*, 2871–2876.

[23] Zhu, H. Y.; Wang, Y.; Xiao, J.; Liu, M.; Xiong, S. M.; Wong, Z. J.; Ye, Z. L.; Ye, Y.; Yin, X. B.; Zhang, X. Observation of piezoelectricity in free-standing monolayer MoS_2. *Nat. Nanotechnol.* **2015**, *10*, 151–155.

[24] Andrei, A.; Krupa, K.; Jozwik, M.; Delobelle, P.; Hirsinger, L.; Gorecki, C.; Nieradko, L.; Meunier, C. AlN as an actuation material for MEMS applications: The case of AlN driven multilayered cantilevers. *Sens. Actuators A: Phys.* **2008**, *141*, 565–576.

[25] Falin, A.; Cai, Q. R.; Santos, E. J. G.; Scullion, D.; Qian, D.; Zhang, R.; Yang, Z.; Huang, S. M.; Watanabe, K.; Taniguchi, T. et al. Mechanical properties of atomically thin boron nitride and the role of interlayer interactions. *Nat. Commun.* **2017**, *8*, 15815.

[26] Zhuang, X. Y.; He, B.; Javvaji, B.; Park, H. S. Intrinsic bending flexoelectric constants in two-dimensional materials. *Phys. Rev. B* **2019**, *99*, 054105.

[27] McGilly, L. J.; Kerelsky, A.; Finney, N. R.; Shapovalov, K.; Shih, E. M.; Ghiotto, A.; Zeng, Y. H.; Moore, S. L.; Wu, W. J.; Bai, Y. S. et al. Visualization of moiré superlattices. *Nat. Nanotechnol.* **2020**, *15*, 580–584.

[28] Chen, Y. C.; Tang, Z. Y.; Shan, H. L.; Jiang, B.; Ding, Y. L.; Luo, X.; Zheng, Y. Enhanced out-of-plane piezoelectric effect in In_2Se_3/transition metal dichalcogenide heterostructures. *Phys. Rev. B* **2021**, *104*, 075449.

[29] Yuan, S. G.; Io, W. F.; Mao, J. F.; Chen, Y. C.; Luo, X.; Hao, J. H. Enhanced piezoelectric response of layered In_2Se_3/MoS_2 nanosheet-based van der Waals heterostructures. *ACS Appl. Nano Mater.* **2020**, *3*, 11979–11986.

[30] Yuan, S. G.; Zhang, Y. M.; Dai, M. Z.; Chen, Y. C.; Yu, H. Y.; Ma, Z. S.; Io, W. F.; Luo, X.; Hou, P. F.; Hao, J. H. A giant tunable piezoelectric performance in two-dimensional In_2Se_3 via interface engineering. *Adv. Electron. Mater.* **2024**, *10*, 2300741.

[31] Cao, V. A.; Kim, M.; Hu, W. G.; Lee, S.; Youn, S.; Chang, J.; Chang, H. S.; Nah, J. Enhanced piezoelectric output performance of the SnS_2/SnS heterostructure thin-film piezoelectric nanogenerator realized by atomic layer deposition. *ACS Nano* **2021**, *15*, 10428–10436.

[32] Kim, J. H.; Lee, J.; Kim, J. H.; Hwang, C. C.; Lee, C.; Park, J. Y. Work function variation of MoS_2 atomic layers grown with chemical vapor deposition: The effects of thickness and the adsorption of water/oxygen molecules. *Appl. Phys. Lett.* **2015**, *106*, 251606.

[33] Tamulewicz, M.; Kutrowska-Girzycka, J.; Gajewski, K.; Serafińczuk, J.; Sierakowski, A.; Jadczak, J.; Bryja, L.; Gotszalk, T. P. Layer

number dependence of the work function and optical properties of single and few layers MoS_2: Effect of substrate. *Nanotechnology* **2019**, *30*, 245708.
[34] Huang, Z. Y.; He, C. Y.; Qi, X.; Yang, H.; Liu, W. L.; Wei, X. L.; Peng, X. Y.; Zhong, J. X. Band structure engineering of monolayer MoS_2 on h-BN: First-principles calculations. *J. Phys. D: Appl. Phys.* **2014**, *47*, 075301.
[35] Joo, M. K.; Moon, B. H.; Ji, H.; Han, G. H.; Kim, H.; Lee, G.; Lim, S. C.; Suh, D.; Lee, Y. H. Electron excess doping and effective Schottky barrier reduction on the MoS_2/h-BN heterostructure. *Nano Lett.* **2016**, *16*, 6383–6389.
[36] Tung, R. T. Recent advances in Schottky barrier concepts. *Mater. Sci. Eng.: R: Rep.* **2001**, *35*, 1–138.
[37] Siao, M. D.; Shen, W. C.; Chen, R. S.; Chang, Z. W.; Shih, M. C.; Chiu, Y. P.; Cheng, C. M. Two-dimensional electronic transport and surface electron accumulation in MoS_2. *Nat. Commun.* **2018**, *9*, 1442.
[38] Hu, Y. X.; Pan, Y. Y.; Wang, Z. L.; Lin, T.; Gao, Y. Y.; Luo, B.; Hu, H.; Fan, F. T.; Liu, G.; Wang, L. Z. Lattice distortion induced internal electric field in TiO_2 photoelectrode for efficient charge separation and transfer. *Nat. Commun.* **2020**, *11*, 2129.
[39] Narvaez, J.; Vasquez-Sancho, F.; Catalan, G. Enhanced flexoelectric-like response in oxide semiconductors. *Nature* **2016**, *538*, 219–221.
[40] Zhang, X. T.; Pan, Q.; Tian, D. X.; Zhou, W. F.; Chen, P.; Zhang, H. F.; Chu, B. J. Large flexoelectriclike response from the spontaneously polarized surfaces in ferroelectric ceramics. *Phys. Rev. Lett.* **2018**, *121*, 057602.
[41] Newnham, R. E.; Skinner, D. P.; Cross, L. E. Connectivity and piezoelectric-pyroelectric composites. *Mater. Res. Bull.* **1978**, *13*, 525–536.
[42] Lozano, H.; Catalán, G.; Esteve, J.; Domingo, N.; Murillo, G. Non-linear nanoscale piezoresponse of single ZnO nanowires affected by piezotronic effect. *Nanotechnology* **2021**, *32*, 025202.